

# Mechanisms of Granule Membrane Recapture following Exocytosis in Intact Mast Cells<sup>\*S</sup>

Received for publication, February 4, 2013, and in revised form, May 7, 2013. Published, JBC Papers in Press, May 24, 2013, DOI 10.1074/jbc.M113.459065

Jose M. Cabeza, Jorge Acosta, and Eva Alés<sup>1</sup>

From the Departamento de Fisiología Médica y Biofísica, Facultad de Medicina, Universidad de Sevilla, 41009 Sevilla, Spain

**Background:** When vesicles undergo exocytosis, the vesicle membrane must be retrieved by endocytosis to maintain a constant cell surface area.

**Results:** Exocytosis in intact mast cells is followed by endocytosis.

**Conclusion:** Mechanisms of granule membrane recapture in intact mast cells include kiss-and-run and “compound endocytosis.”

**Significance:** Compound endocytosis may be a novel mechanism for efficiently compensating for the membrane excess caused by exocytosis.

In secretory cells, several exocytosis-coupled forms of endocytosis have been proposed including clathrin-mediated endocytosis, kiss-and-run endocytosis, cavicapture, and bulk endocytosis. These forms of endocytosis can be induced under different conditions, but their detailed molecular mechanisms and functions are largely unknown. We studied exocytosis and endocytosis in mast cells with both perforated-patch and whole-cell configurations of the patch clamp technique using cell capacitance measurements in combination with amperometric serotonin detection. We found that intact mast cells exhibit an early endocytosis that follows exocytosis induced by compound 48/80. Direct observation of individual exocytic and endocytic events showed a higher percentage of capacitance flickers (27.3%) and off-steps (11.4%) in intact mast cells than in dialyzed cells (5.4% and 2.9%, respectively). Moreover, we observed a type of endocytosis of large pieces of membrane that were likely formed by cumulative fusion of several secretory granules with the cell membrane. We also identified “large-capacitance flickers” that occur after large endocytosis events. Pore conductance analysis indicated that these transient events may represent “compound cavicapture,” most likely due to the flickering of a dilated fusion pore. Using fluorescence imaging of individual exocytic and endocytic events we observed that granules can fuse to granules already fused with the plasma membrane, and then the membranes and dense cores of fused granules are internalized. Altogether, our results suggest that stimulated exocytosis in intact mast cells is followed by several forms of compensatory endocytosis, including kiss-and-run endocytosis and a mechanism for efficient retrieval of the compound membrane of several secretory granules through a single membrane fission event.

During exocytosis, the membrane surrounding a cytosolic vesicle fuses with the plasma membrane, and the contents of the vesicle are released into the extracellular space. After exocytosis, the membrane must be retrieved by endocytosis to maintain a constant cell surface area and allow the secretory vesicle to recycle (1, 2). Therefore, efficient endocytosis is crucial for preventing the complete exhaustion of secretory vesicles and also to help maintain normal cell morphology by retrieving excess membrane. Three forms of endocytosis have been identified: clathrin-mediated slow endocytosis, kiss-and-run endocytosis, and bulk endocytosis. During clathrin-mediated endocytosis, clathrin-coated invaginations of the surface membrane are internalized, and the clathrin coat is removed before the next round of exocytosis (3–5). The kiss-and-run model proposes that vesicles do not fully collapse into the surface membrane but recycle rapidly after closure of a fusion pore that allows escape of the transmitter (6, 7). A related mechanism referred to as granule cavity recapture (cavicapture) or granule recapture posits that the fusion pore dilation allows the loss of cargo and some membrane components while the omega shape of the fusing granule is preserved (8–10). Bulk endocytosis, a phenomenon in which a large piece of the plasma membrane is retrieved, has also been frequently observed in several model cells, including the frog neuromuscular junction (11), rat hippocampal neurons (12), and goldfish bipolar cells (13). The mechanisms by which exocytosis and endocytosis are functionally coupled are the subject of much controversy, possibly because of the multiple kinetic components that are involved, each with different underlying mechanisms.

At present, two types of electrophysiological recordings are commonly used to monitor exocytosis at the single-cell level. Capacitance measurements of the membrane surface area are effectively used to follow vesicle exocytosis and endocytosis (14, 15). When vesicles fuse with the plasma membrane, the surface area of the plasma membrane increases, thereby increasing membrane capacitance. Therefore, an increase in capacitance indicates exocytosis, whereas a decrease indicates endocytosis (16, 17). Changes in fusion pore conductance are also used as criteria when distinguishing between the kiss-and-run and full-collapse models. A rapid opening and closing of the fusion pore

\* This work was supported by the Ministerio de Ciencia e Innovación ISCIII and Fondos FEDER Grant PI11/00257 (to E. A.).

<sup>S</sup> This article contains supplemental Fig. 1S and Videos 1 and 2.

<sup>1</sup> To whom correspondence should be addressed: Dpto. Fisiología Médica y Biofísica, Facultad de Medicina, Universidad de Sevilla, Av. Sánchez Pizjuán 4, 41009 Sevilla, Spain. Tel.: 34-954559868; Fax: 34-954551796; E-mail: eales@us.es.

## Granule Recapture in Intact Mast Cells

indicates kiss-and-run fusion, whereas fusion pore opening followed by expansion indicates full-collapse fusion. An alternative method of measuring secretion is by monitoring the release of oxidizable secretory products, observed as brief current spikes, by placing a carbon fiber microelectrode in close proximity to an isolated cell (18). Combined amperometric and capacitance measurements have shown that the detection of a single amperometric spike corresponds to the fusion of a single granule with the plasma membrane (7, 19, 20). One advantage of this method of secretion measurement is that it monitors only the release of secretory products into the extracellular milieu and, therefore, is not complicated by many of the factors affecting capacitance measurements.

Pioneering information supporting kiss-and-run endocytosis was obtained from membrane capacitance assays performed in mast cells and chromaffin cells (7, 21). Most of the capacitance studies so far have been performed in the whole-cell recording mode with patch pipettes. In this configuration, small molecules can diffuse freely between the cell and the recording pipette, potentially depleting or "washing out" important regulatory components, such as second messengers and small soluble proteins. The perforated-patch technique avoids this problem (22). The aim of the present work was to determine whether cytosolic factors are required for exocytic-endocytic coupling and to investigate the mechanisms that maintain a balance between exocytosis and endocytosis, allowing tight control of the membrane surface area. We have studied exocytosis and endocytosis in mouse peritoneal mast cells at the single-vesicle level using perforated-patch capacitance measurements and amperometry together with fluorescence imaging. Our results suggest the existence of two modes of rapid compensatory endocytosis: kiss-and-run endocytosis, where a single vesicle fuses transiently with the plasma membrane through a narrow fusion pore to release the transmitters that it contains, and "compound endocytosis," where a granule aggregate formed by cumulative fusion is disconnected from the plasma membrane through a fission pore.

### EXPERIMENTAL PROCEDURES

**Cell Preparation, Reagents, and Solutions**—Peritoneal mouse mast cells were obtained from 2–3-month-old animals as described previously (23). Mice were euthanized according to ethical procedures and exsanguinated. Extraction solution (3 ml) was injected into the peritoneal cavity. After 2 min of gentle abdominal massage, the peritoneal cavity was surgically exposed, and 1–2 ml of fluid was recovered. Subsequently, the cell suspension was centrifuged at 200 *g* for 2 min. The pellet was resuspended in 1 ml of extraction solution. Cells were plated on coverslips and incubated at 37 °C in an atmosphere of 5% CO<sub>2</sub> and 95% air until use (between 1 and 6 h after culture). All experiments were carried out at 22–25 °C. The external medium comprised the following components: 140 mM NaCl, 10 mM HEPES, 3 mM KOH, 2 mM Cl<sub>2</sub>Mg, and 1 mM Cl<sub>2</sub>Ca. Glucose was added to adjust the osmolarity to 310 mOsmol·kg<sup>-1</sup>.

For the perforated-patch configuration, we used compound 48/80 as a secretagogue. Patched cells that exhibited sufficient access conductance and a low level of leakage were stimulated

by pressure ejection (PDES-02DX, npi electronic GmbH, Scientifica) for 5 s with compound 48/80 solution from a puffer pipette positioned near the cell under study.

**Electrophysiological Recordings**—Electrophysiological recordings in this study were performed in the whole-cell and perforated-patch configurations. The whole-cell pipette solution contained the following components: 140 mM potassium glutamate, 10 mM HEPES, 7 mM MgCl<sub>2</sub>, 3 mM KOH, 0.2 mM Mg-ATP, 7.5 mM Ca<sup>2+</sup>-EGTA, and 2.5 mM K<sub>2</sub>-EGTA. The final Ca<sup>2+</sup> concentration was 320 nM. We added 1 μM GTPγS<sup>2</sup> to the pipette solution to induce degranulation. Degranulation occurs spontaneously and reproducibly if Mg-ATP and the GTP analog GTPγS are present in the pipette-filling solution (15). The perforated-patch pipette solution contained 135 mM Cs-glutamate, 10 mM HEPES, 9.5 mM NaCl, 0.5 mM tetraethylammonium chloride, and 0.5 mM amphotericin B; the solution was adjusted to pH 7.2 with CsOH. All chemicals were obtained from Sigma with the exception of amphotericin B (Calbiochem-Novabiochem). An amphotericin B stock solution was prepared daily at a concentration of 50 mg/ml in dimethyl sulfoxide and kept protected from light. The final concentration of amphotericin B was prepared by ultrasonication in the darkness 10 μl of stock amphotericin B in 1 ml of Cs-glutamate internal solution. Pipettes were tip-dipped in amphotericin-free solution for several seconds and back-filled with freshly mixed amphotericin intracellular solution. Pipettes of 2–5-megohm resistance were pulled from borosilicate glass capillary tubes, fire-polished, and partially coated with wax. Patched cells were allowed to perforate to less than 30-megohm series resistance prior to recording.

Whole-cell and perforated-patch capacitance were measured with a lock-in amplifier (SR-830; Stanford Research Instruments). The C-slow and G-series potentiometers of an EPC-7 patch clamp amplifier (Heka Electronics) were used to cancel out the incoming membrane current to resolve small-capacitance changes. We obtained a calibration signal by unbalancing the C-slow potentiometer by 100 fF, which corresponds to a change of 10 μm<sup>2</sup> (assuming a specific membrane capacitance of 1 μF·cm<sup>-2</sup>). We set the phase manually at the beginning of each recording. The V-command was a 50-mV sine wave (root mean square, 1 kHz). The data acquisition was performed with a 16-bit A/D converter (6052-E; National Instruments) with locally written software in Igor Pro (Wavemetrics, Inc.). One data point was obtained every millisecond.

**Electrochemistry**—Amperometric detection of serotonin was monitored with a carbon fiber microelectrode with a tip diameter of 12 μm, fabricated as described elsewhere (24). Electrodes were backfilled with a 3 M KCl solution. The holding voltage applied to the electrode was 650 mV, and the redox current was monitored with an EPC-8 patch clamp amplifier (Heka Electronics). Carbon fiber was cut fresh prior to each recording and placed in close proximity to the cell.

**Imaging**—Imaging experiments were done with a system comprising an Axiovert 200 inverted microscope, a

<sup>2</sup> The abbreviations used are: GTPγS, guanosine 5'-O-(γ-thio)triphosphate; F, farads (fF, pF); G<sub>p</sub>, pore conductance; Im, imaginary; Re, real; S, siemens; C, coulomb (pC).

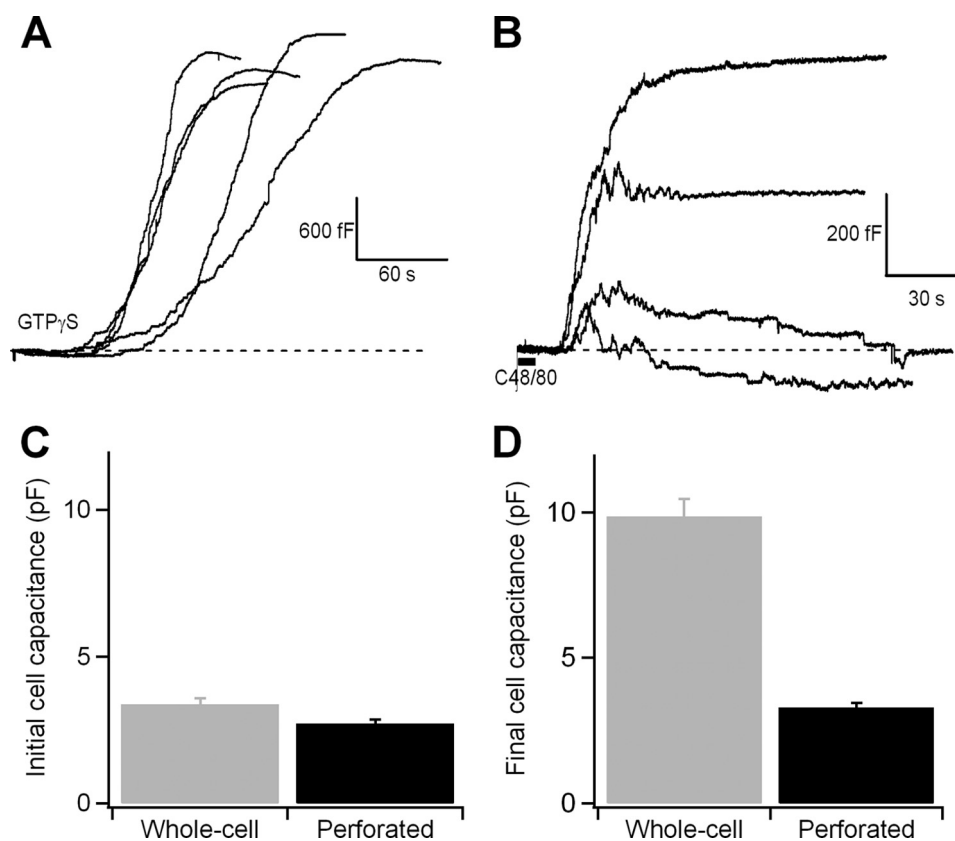


**FIGURE 1. Exocytosis is measured as an increase in the cell membrane capacitance caused by the addition of the secretory granule membrane.** *A* and *B*, time courses of capacitance of the cell membrane during degranulation, recorded in the whole-cell configuration (the patch pipette contained the standard internal solution plus  $1 \mu\text{M}$   $\text{GTP}\gamma\text{S}$ ) (*A*) and during compound 48/80-mediated degranulation, recorded in the perforated-patch configuration (*B*). *C*, overall starting capacitance in mast cells before stimulation of exocytosis with  $\text{GTP}\gamma\text{S}$  (whole-cell) and compound 48/80 (perforated-patch). *D*, overall final exocytosis in mast cells after stimulation of exocytosis with  $\text{GTP}\gamma\text{S}$  (whole-cell) and compound 48/80 (perforated-patch). Error bars, S.E.

Hamamatsu ORCA-R2 camera ( $6.45 \times 6.45 \mu\text{m}$  physical pixels, giving  $102 \text{ nm/image pixel}$  with a  $63\times$  oil immersion objective) and a HCSImage software (Hamamatsu Photonics). Fluorescence images of FM1-43-stained cells were obtained with a standard filter set (XF115-2; Omega Optical). Exposures lasted  $0.2 \text{ s}$ , and images were acquired at  $\sim 1 \text{ Hz}$ . External solutions were exchanged by a fast superfusion device consisting of a multibarreled pipette, the common outlet of which was positioned  $50\text{--}100 \mu\text{m}$  from the cell. Standard and FM1-43 solutions were changed using a pinch valve controller system (Warner Instruments) manipulated by a manual switch. The flow rate ( $0.5\text{--}1 \text{ ml}\cdot\text{min}^{-1}$ ) was regulated by gravity to achieve a complete replacement of cell surroundings in  $<2 \text{ s}$ . All experiments were performed at room temperature ( $22\text{--}24 \text{ }^\circ\text{C}$ ). Quantitative analyses were performed on raw images. Fluorescence images were analyzed using HCSImage (Hamamatsu Photonics) and Igor Pro (Wavemetrics, Inc.). The spots for fluorescence analysis were selected by the threshold brightness (usually 80% of the difference between the brightness and dimmest pixels). Exceeding this threshold, most of fluorescent spots were detected. Isolated mast cells were bathed in solution containing  $4 \mu\text{M}$  FM1-43 and stimulated with a solution containing compound 48/80 ( $100 \mu\text{g/ml}$ ) and  $4 \mu\text{M}$  FM1-43 for  $10 \text{ s}$ , which induces a massive vesicular fusion to the plasma membrane. Once the degranulation stopped ( $\sim 3\text{--}4 \text{ min}$ ), extracellular FM1-43 was washed out with standard solution for at least  $4$

min. Some experiments were conducted in the presence of Advasep-7 to decrease the FM1-43 background.

**Data Analysis**—Data analysis was performed using macros for Igor (Wavemetrics, Inc.). We analyzed the steps from each exocytic and endocytic event. Each step reflects the area of a retrieved or fused vesicle. Vesicle radii were calculated assuming that a vesicle is spherical and that the specific membrane capacitance of the vesicle is  $1 \mu\text{F}\cdot\text{cm}^{-2}$ . Pore conductance ( $G_p$ ) was calculated from the real (Re) and imaginary (Im) parts of the admittance after base-line subtraction:  $G_p = (\text{Re}^2 + \text{Im}^2)/\text{Re}$ .  $G_p$  was used to estimate the fission pore diameter (25, 26):  $D_p = (4\rho L/\pi)^{0.5} G_p^{0.5}$ . For analysis of the quantal charge of amperometric spikes, only those events that were not overlapping were included. Statistical significance was tested using SPSS Statistics 20.0 software with a two-tailed nonparametric Mann-Whitney test (samples were considered significantly different when  $p \leq 0.05$ ). All data are expressed as the means  $\pm$  S.E.

## RESULTS

### Rapid Endocytosis following Exocytosis in Intact Mast Cells—

The increase in cell surface area that occurs when secretory granules fuse with the plasma membrane can be observed as an increase in membrane capacitance with the patch clamp technique. Fig. 1*A* shows the time courses of the membrane capacitance changes caused by the fusion of several hundred secre-



## Granule Recapture in Intact Mast Cells

tory granules (23) in mouse peritoneal mast cells. The cells were stimulated by  $1 \mu\text{M}$  GTP $\gamma\text{S}$  contained in the pipette solution. The recordings show the cell membrane capacitance as a function of time starting when the cell perfusion was initiated. In each cell, the membrane area begins to expand after a lag period, and degranulation proceeds to a similar shape and extent, consistent with previous reports (15, 27, 28). However, it has been shown that dialyzed cells fail to respond to external stimuli such as compound 48/80 or antigens, whereas intact cells degranulate within several minutes (29), suggesting that essential cytoplasmic components have been washed out. To determine whether cytosolic factors affect the properties of membrane fusion and fission, we performed experiments in the perforated-patch recording mode, in which the patch under the pipette tip is not disrupted but instead permeabilized, preventing the diffusion of small molecules out of the cell. In this configuration, 34 of 56 cells showed changes in membrane capacitance several seconds after the application of compound 48/80 with a puffer pipette; 15 cells were silent, and 7 cells showed spontaneous responses before drug application. Fig. 1B shows various time courses of changes in the cell membrane capacitance following stimulation with compound 48/80. Initially, an abrupt increase in capacitance, indicating exocytosis, was observed; this increase was followed by a variable decrease in capacitance, indicating endocytosis. In some recordings, exocytosis was tightly compensated by endocytosis, maintaining the initial membrane surface area, even the capacitance may have overshoot the base line. If we express our individual experiment values as percentages of the initial whole-cell capacitance, 30.8% of cells were able to return to basal capacitance values, 38.5% of cells increased their final capacitance between the 3 and 9%, and 30.8% increased their final capacitance above 10% of the basal. We next quantified and compared the overall capacitance changes that were triggered by GTP $\gamma\text{S}$  and compound 48/80. Cells exhibited a similar overall initial capacitance in the whole-cell configuration ( $3.38 \pm 0.2$  pF;  $n = 22$  cells) and the perforated-patch mode ( $2.71 \pm 0.14$  pF;  $n = 26$  cells) (Fig. 1C). Notably, however, the final capacitance differed between the recording modes ( $9.86 \pm 0.6$  pF in the whole-cell mode;  $3.29 \pm 0.16$  pF in the perforated-patch mode) (Fig. 1D). The extents of degranulation, expressed as the ratio of the final and initial capacitance ( $C_f/C_i$ ) were 2.91 (GTP $\gamma\text{S}$ ) and 1.21 (compound 48/80). The response obtained with GTP $\gamma\text{S}$  was similar to that obtained previously under similar conditions (28, 30, 31). The results observed with compound 48/80 in intact mast cells evidence mechanisms of early endocytosis following exocytosis which assist in maintaining a suitable membrane area surface.

Amperometry provides another powerful real-time method, complementary to capacitance measurements, that allows the electrochemical detection of oxidizable secretory products (18). The release of the secretory granule contents results in the generation of brief current spikes as the secretory products are oxidized on the surface of the carbon fiber (18). Serotonin is the main secretory product detected in peritoneal mast cells by amperometry (7). Fig. 2 shows combined membrane capacitance (*blue traces*) and amperometry (*red traces*) measurements of exocytosis induced by compound 48/80 (perforated-

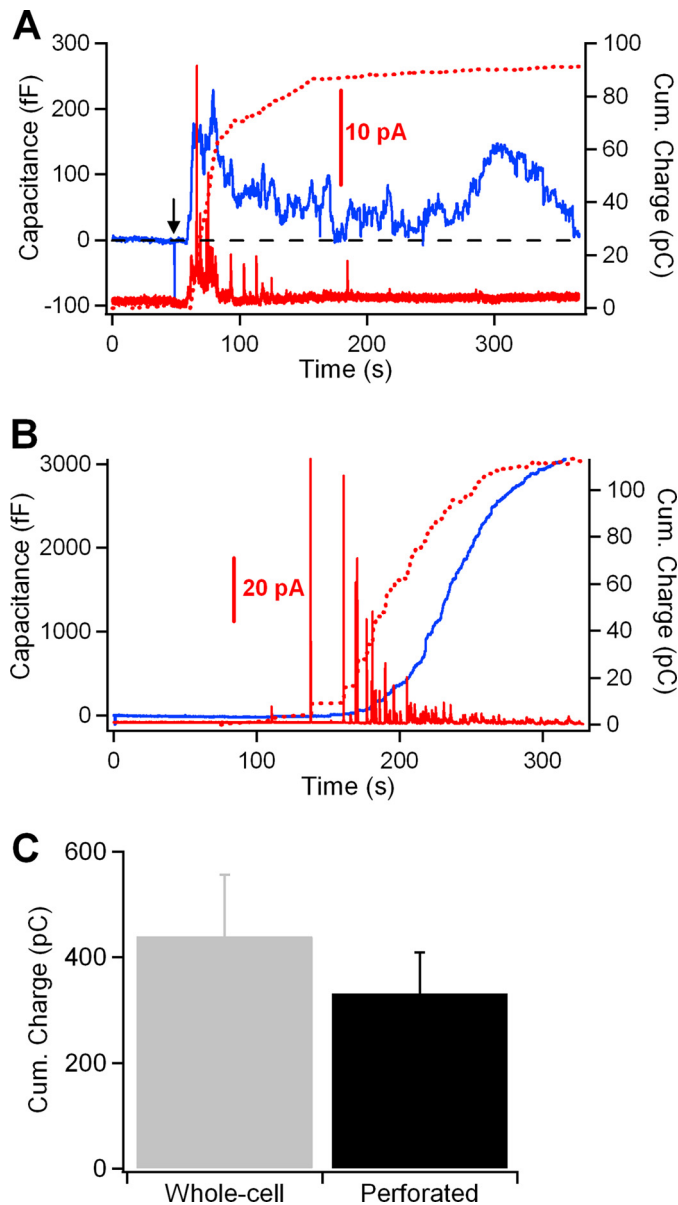
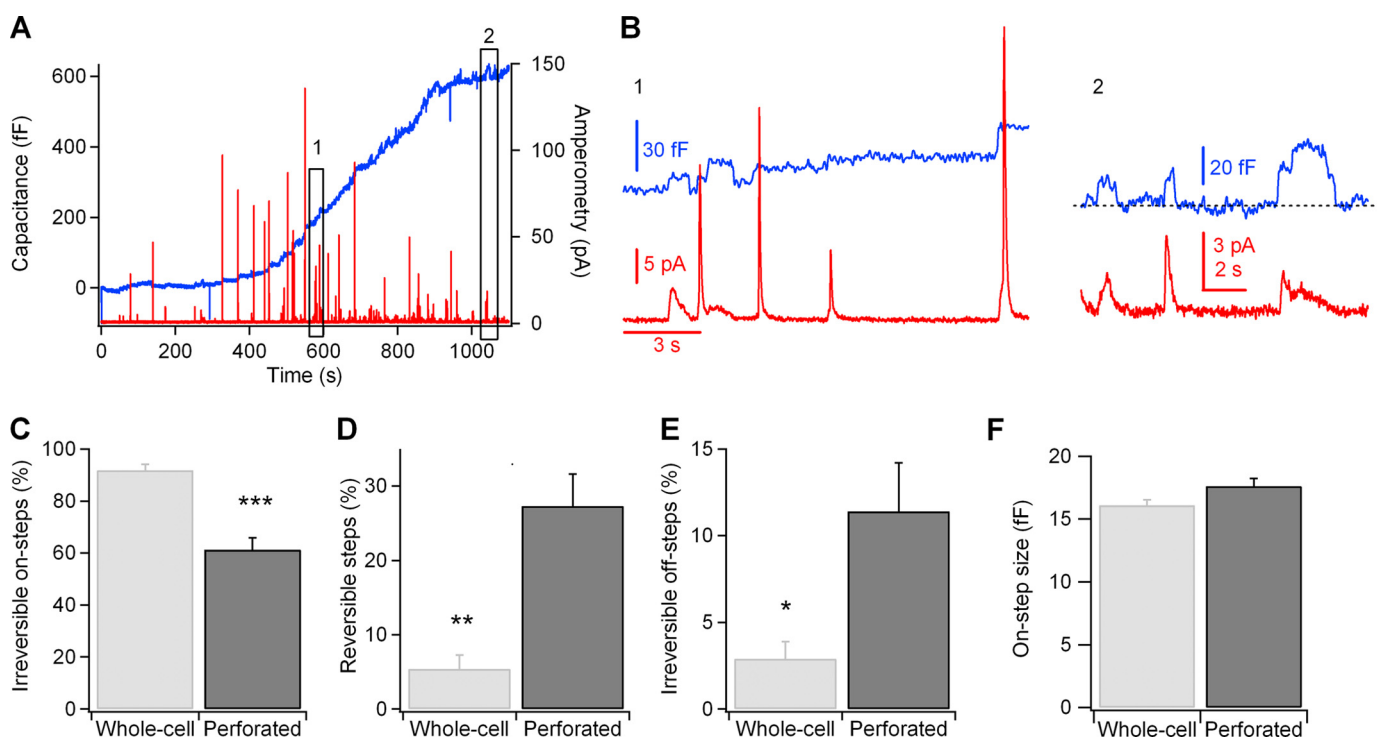


FIGURE 2. *A* and *B*, simultaneous cell membrane capacitance (*blue trace*) and amperometric (*red trace*) measurements of exo-endocytosis in mast cells under the perforated-patch (*A*) and whole-cell (*B*) configurations. The time integrals of the amperometric traces are shown as a *dotted line* superimposed on the cell membrane capacitance traces and represent the total amount of serotonin detected by the carbon fiber during the secretory response. Secretion was stimulated by a puff (5 s) of compound 48/80 (100  $\mu\text{g}/\text{ml}$ ) (*arrow*) in intact mast cells and by adding  $1 \mu\text{M}$  GTP $\gamma\text{S}$  to the patch pipette solution in the whole-cell experiments. *C*, average cumulative charge of serotonin in whole-cell and perforated-patch recordings. *Error bars*, S.E.

patch) (Fig. 2A) and GTP $\gamma\text{S}$  (whole-cell) (Fig. 2B). Despite a null net increase in membrane capacitance in the cell shown in Fig. 2A, a burst of amperometric spikes was observed during the initial phase of response. This fact is better observed by integrating the amperometric recording over the duration of the membrane capacitance recording. The time integral of the amperometric trace is a measure of the total amount of secretory products released by a cell after its stimulation and, therefore, allows a direct comparison of the events measured by amperometry with those measured by capacitance (19, 20, 32). In response to a GTP $\gamma\text{S}$  stimulus, the integral of the ampero-



**FIGURE 3. Secretory responses in an intact mast cell.** *A*, the cell membrane capacitance (blue trace) was measured simultaneously with the amperometric current (red trace). *B*, perforated-patch recordings and simultaneously recorded amperometric signals from mast cells showed spontaneous single-vesicle capacitance steps and amperometric spikes. *C–E*, percentage of irreversible on-steps (*C*), reversible steps (*D*), and irreversible off-steps (*E*) were significantly different in whole-cell and perforated-patch recordings (\*\*\*,  $p = 0.00005$ ; \*\*,  $p = 0.001$ ; \*,  $p = 0.035$ ). *F*, the size of the capacitance steps induced by exocytosis of individual granules was similar for cells under the whole-cell and perforated-patch configurations ( $p > 0.05$ ). Error bars, S.E.

metric current recording followed a sigmoidal time course similar to that of the capacitance measurement (dotted red line, Fig. 2*B*). The secretory response elicited by external stimulation in intact mast cells showed that the initial increase in the capacitance trace was closely correlated with the time integral of the amperometric current trace (dotted red line, Fig. 2*A*). During the phase of membrane retrieval, however, significant secretion from the cell was not evident from the amperometric recording. Interestingly, the integrated amperometric charge was comparable under both recording modes ( $439 \pm 117$  pC,  $n = 10$  cells in whole-cell;  $331 \pm 78$ ,  $n = 13$  cells in perforated-patch; Fig. 2*C*). These results suggest that following a robust exocytosis in intact cells, compound 48/80 elicited a rapid reuptake of plasma membrane.

**High Incidence of Capacitance Flickers and Endocytosis in Intact Mast Cells**—Measurements of changes in cell membrane capacitance caused by the fusion or the fission of a granule make it possible to obtain time-resolved recordings of exocytosis and endocytosis at the level of single granules. In addition, the size of the granules can be determined by capacitance measurements in mast cells because of the large size of the granules secreted by these cells. A drawback of the abrupt response in cell membrane capacitance measured in intact mast cells under stimulation with compound 48/80 is that individual fusion and fission events are not clearly resolved because there are many overlapping events. Fig. 3*A* shows the changes in cell membrane capacitance and serotonin release measured in an intact mast cell in which exocytosis occurred spontaneously and the rate of fusion was sufficiently low for the capacitance changes to

occur in discrete steps. Fig. 3*B* shows two types of fusion events: irreversible step increases in membrane capacitance correlated with amperometric spikes and transient increases in capacitance (flickers) that are also correlated with small amperometric spikes. The first type of event represents the abrupt and irreversible opening of the fusion pore, and the latter event represents the opening and subsequent closure of the fusion pore. Inspection of capacitance traces in the perforated-patch configuration, both from spontaneous experiments and from experiments where compound 48/80 produced a lower rate of degranulation, indicated that there may be an increase in the frequency of capacitance flickers (transient fusion events) and endocytosis compared with that observed during the initial phase of the degranulation in cells stimulated by GTP $\gamma$ S under the whole-cell configuration (Fig. 3, *C–E*). The percentage of transient fusion events measured in intact mast cells was  $\sim 5$  times larger than in dialyzed cells ( $27.3 \pm 4.3$  and  $5.4 \pm 1.9$ , respectively) (Fig. 3*D*). The percentage of fission events (irreversible off-steps) was also  $\sim 4$  times larger in intact ( $11.4 \pm 2.8$ ) than in dialyzed mast cells ( $2.9 \pm 1$ ) (Fig. 3*E*). The average size of the individual capacitance steps was similar in intact ( $17.6 \pm 0.62$  fF;  $n = 642$ ) and dialyzed mast cells ( $16.1 \pm 0.45$  fF;  $n = 318$ ) (Fig. 3*F*). Therefore, the decrease in the overall capacitance change in intact mast cells after stimulation with compound 48/80 may be explained by the tendency to undergo more frequent fusion reversals and irreversible fission events after exocytosis but not by the fusion of smaller secretory granules.

## Granule Recapture in Intact Mast Cells

**TABLE 1**  
Properties of small and large flickers in intact mast cells

Property	Small flickers	Large flickers
Frequency (%)	27.3	Occasional
Step size (fF)	14.9 ± 0.5	72.3 ± 3.7
Duration (s)	1.5 ± 0.1	7.8 ± 2.8
Pore conductance (nS)	0.39 ± 0.03	2.91 ± 0.39
Pore diameter (nm)	2.4 ± 0.7	6 ± 1
Charge (pC)	1.5 ± 0.2	

*Two Phenotypes of Granule Recapture in Perforated-patch Experiments*—We further analyzed capacitance flickers in intact mast cells. As mentioned, we observed a large increase in the incidence of capacitance flickers in which the capacitance increase was rapidly reversed but still associated with an amperometric signal (Figs. 3*B* and 4, *A* and *B*, *arrows*). Our capacitance recordings showed capacitance flickers with sizes in the on-step range (Fig. 4*C*) ( $14.9 \pm 0.54$  fF;  $n = 251$ ). The on- and off-steps within each capacitance flicker were closely correlated in size, with linear regression slopes close to one (slope = 0.94) (Fig. 4*E*, *lined red circles*). This mechanism of compensatory endocytosis, which suggests the retrieval of single granules, was proposed decades ago for mast cells (7, 15) and is referred to as a kiss-and-run event (33). Moreover, we occasionally observed “large-capacitance flickers” immediately after an irreversible off-step of similar size without any associated amperometric response (Fig. 4, *A* and *B*, *asterisks*). These large flickers showed step sizes in the range of irreversible off-steps (Fig. 4*D*). Two populations of endocytic events have been proposed to exist in mast cells (34). The first population of endocytic events is similar in size to the exocytic events (<60 fF); therefore, it is most likely caused by the retrieval of single granules. A second population of events (>60 fF) is too large to be accommodated by the retrieval of individual granules. Large-capacitance flickers are within the size range of large off-step events ( $72.4 \pm 3.7$  fF;  $n = 15$ ). Although the on- and off-steps within each large-capacitance flicker were closely correlated in size (Fig. 4*E*, *filled red circles*), several of the on- and off-steps clearly differed from each other in size (Fig. 4*B*). Amperometry allows us to determine the quantal release of serotonin associated with these events (Fig. 4*F*). The mean ± S.E. spike charge was  $2.2 \pm 0.2$  pC ( $n = 105$ ) in the full-fusion events and  $1.5 \pm 0.2$  pC ( $n = 45$ ) in the small-capacitance flickers. However, no serotonin release was detected in association with the large flickers. Fig. 4*G* plots the relationship between the amplitude of capacitance increases and the amplitude of the amperometric spikes. The *black dots* represent full-fusion events, and the *lined red dots* show the same relationship for transient fusion events (small flickers). Note that the charge of the spikes for which the change in capacitance was reversible was smaller, on average, than that of spikes where an irreversible capacitance change was observed. The amount of serotonin released during kiss-and-run events was significantly smaller than in full-fusion events, further indicating partial release of the vesicle contents through a small fusion pore. We plotted the frequency distribution of flickers lifetime (Fig. 4*H*). The distribution followed an approximately exponential distribution with a time constant of  $5.6 \pm 0.06$  s. The properties of small and large flickers in intact mast cells are shown in Table 1.

Changes in fusion pore conductance can be used as criteria when distinguishing between the kiss-and-run and full-collapse models. During capacitance flickers, simultaneous changes can be observed in both the imaginary (Im, *blue traces* in Fig. 5) and real (Re, *green traces*) signals of the lock-in amplifier, and these signals can be used to calculate the fusion pore conductance ( $G_p$ ) (see “Experimental Procedures”).

In the typical exocytic event shown in Fig. 5*A*, the fusion pore had an initial conductance of 600 pS (*yellow, bottom trace*), which increased to  $\sim 1.5$  nS in the next 500 ms and then increased steeply to a conductance exceeding 7 nS. During most of the flickers shown in Fig. 5, *B* and *C*, the fusion pore conductance remained at  $\sim 600$  pS. The fusion pore diameter can be estimated from the conductances associated with these exocytic and flicker events (see “Experimental Procedures”). The initial pore diameter from the exocytic events ( $2.4 \pm 0.4$  nm;  $n = 30$ ) was similar to the mean pore diameter obtained from the flicker events ( $2.4 \pm 0.7$ ;  $n = 13$ ) (Fig. 5*D*). Next, we plotted the frequency distribution of  $G_p$  values measured during fusion pore expansion in exocytic (Fig. 5*E*) and flicker events (Fig. 5*F*). The frequency distribution of  $G_p$  values of full-fusion events shows that the pore conductances exceeded 2 nS, indicating a complete pore collapse. However, during transient fusion events, the distribution of  $G_p$  was shifted to smaller conductance values (<2 nS). As previously published, we conclude that these flickers are characterized by the partial and transient opening of fusion pores from secretory granules (7).

Off-steps that were not preceded by on-steps presumably reflect endocytosis that is not coupled to exocytosis, and during these transitions, we occasionally detected fission pores. For large events such as that shown in Fig. 6*A*, closing of the fission pore could be analyzed. This example shows a closure that occurred from a conductance of 7 nS and lasted  $\sim 800$  ms. Analysis of the  $G_p$  revealed that the time course could be better fitted to a double-exponential function (data not shown), reflecting that the decrease in  $G_p$  occurred in phases. In the initial phase, the conductance decreases rapidly from 7 to 3 nS for  $\sim 50$  ms. This phase is followed by a slower decrease with an overall slope of 6 pS/ms, and in the final phase,  $G_p$  decreases more steeply. These dynamics have been proposed to be generated as a result of a constriction and lengthening of the fission pore (34). The capacitance recordings also contained large-capacitance flickers preceded by off-steps. Both the on- and off-steps were accompanied by transient changes in conductance indicating the formation of fusion and fission pores (Fig. 6*B*). The conductance of the fusion pore was 600 pS when opened and subsequently grew to nearly 8 nS. Clearly, the pore conductances reached during large-capacitance flickers are much greater than typical conductance values observed for transient pores. Later ( $\sim 800$  ms), a slow closure occurred from a conductance of 8 nS and proceeded at a similar rate as it developed in typical endocytic fission pores, indicating that during large-capacitance flickers, a fusion pore can dilate and close again completely. A frequency histogram of the pore conductance values observed during these capacitance flickers, from 12 different events similar to those in Fig. 6*B*, is shown in Fig. 6*D* and is quite similar to the conductance histogram of irreversible fission events (Fig. 6*C*). Consistent with this observation, the



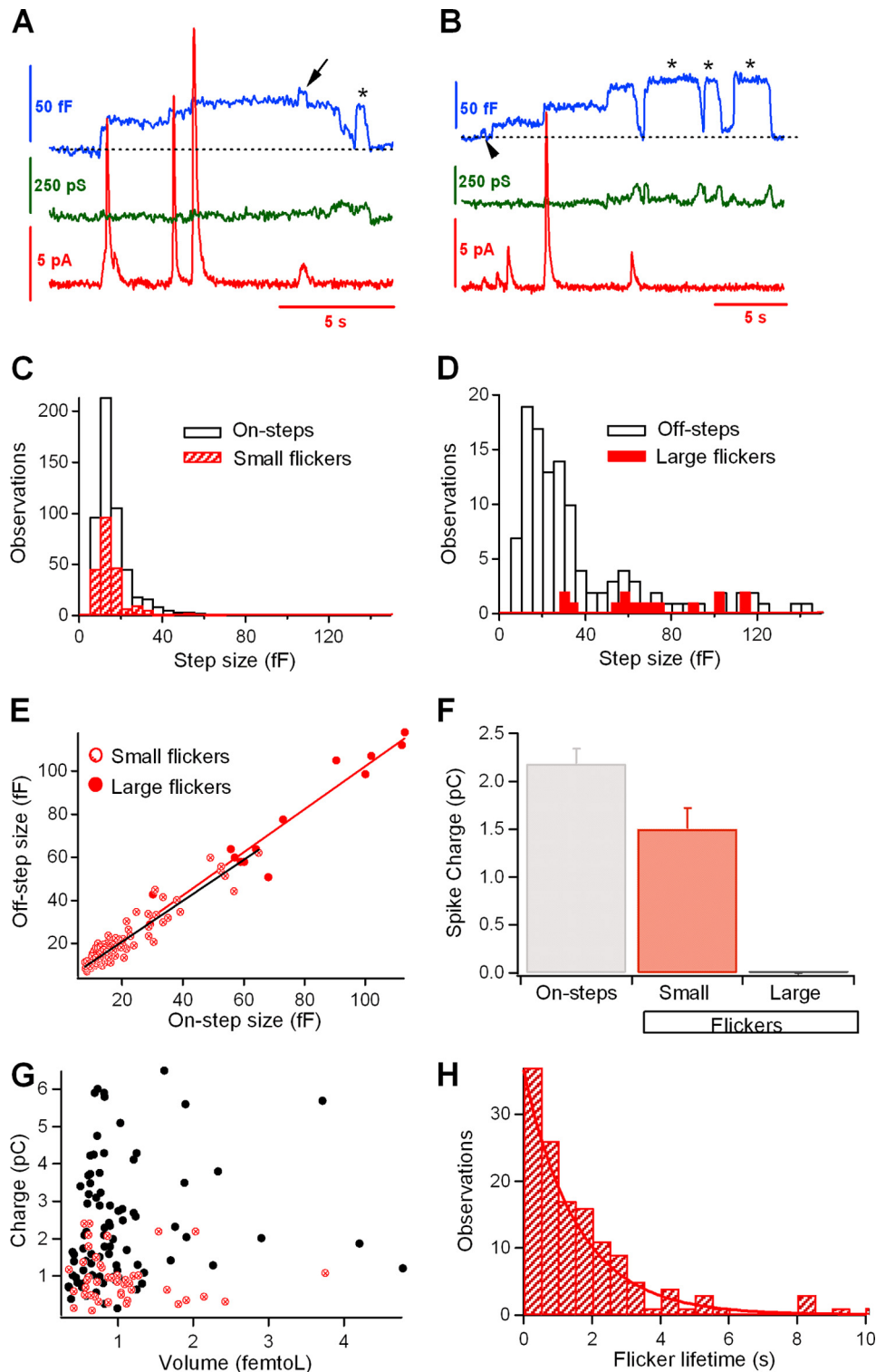


**FIGURE 4. Two phenotypes of granule recapture in perforated-patch experiments.** *A* and *B*, recordings showing two types of capacitance flickers: small (arrows) and large (asterisks). *C* and *D*, distributions of capacitance step size of small flickers in relation to irreversible on-steps (*C*) and of large flickers in relation to irreversible off-steps (*D*). *E*, correlation between on- and off-step size in small (lined red circles) and large (filled red circles) flickers. *F*, average charge of amperometric spikes associated with on-steps and small and large flickers. *G*, relationship between amperometric spike charge and vesicle volume as calculated from the change in capacitance. Black dots represent step changes in capacitance; lined red dots represent the capacitance increase during small-capacitance flickers. *H*, lifetime distribution of small-capacitance flickers with  $\tau$  of 5.6 s. Error bars, S.E.

average pore conductance during the fission of reversible events was  $2.9 \pm 0.39$  nS; this value is comparable with the pore conductance observed during typical endocytosis ( $2.2 \pm 0.17$  nS;  $n = 33$ ). Furthermore, the lifetimes of fusion and fission

pores in reversible and irreversible events were similar (irreversible on-step,  $140 \pm 5.4$  ms; reversible on-step,  $199 \pm 53$  ms; irreversible off-step,  $1056 \pm 53$  ms; reversible off-step,  $947 \pm 308$  ms) (Fig. 6*E*). Therefore, the fusion and fission pore time

## Granule Recapture in Intact Mast Cells

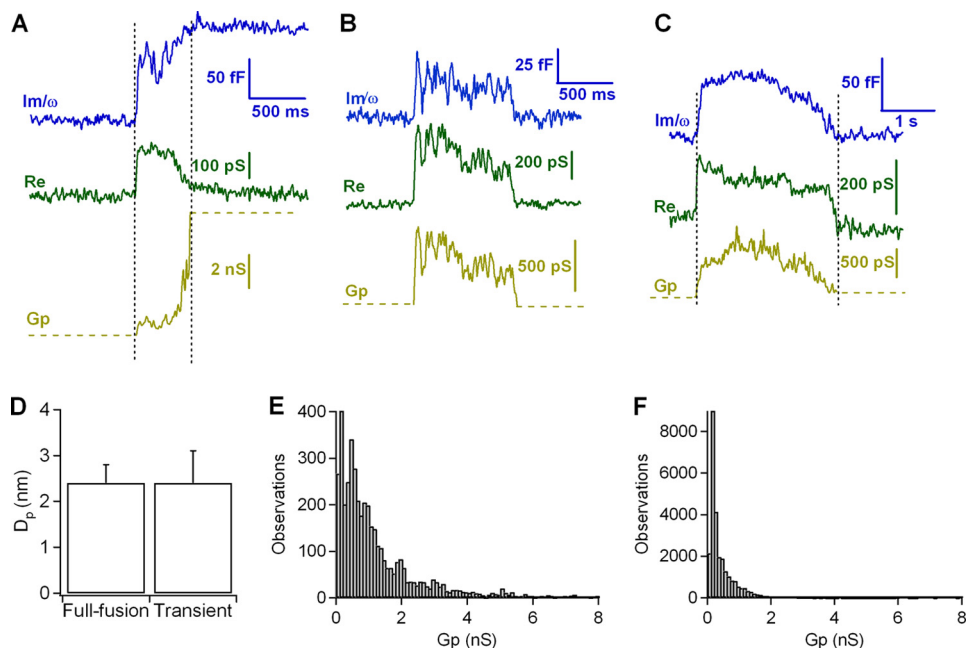


FIGURE 5. A–C, analysis of fusion pores from irreversible (A) and reversible (B and C) fusion events. The imaginary part ( $Im/\omega$ , blue trace) increases gradually before reaching full vesicle capacitance, whereas the real part ( $Re$ , green trace) shows a transient increase. The fusion pore conductance ( $G_p$ , yellow trace) was calculated from the real and imaginary traces (see “Experimental Procedures”). D, initial fusion pore diameter of full fusion events and mean pore diameter of transient events. Error bars, S.E. E and F, frequency distribution of  $G_p$  values during fusion-pore expansion of full fusion events (E) and during pore formation of transient fusion events (F).

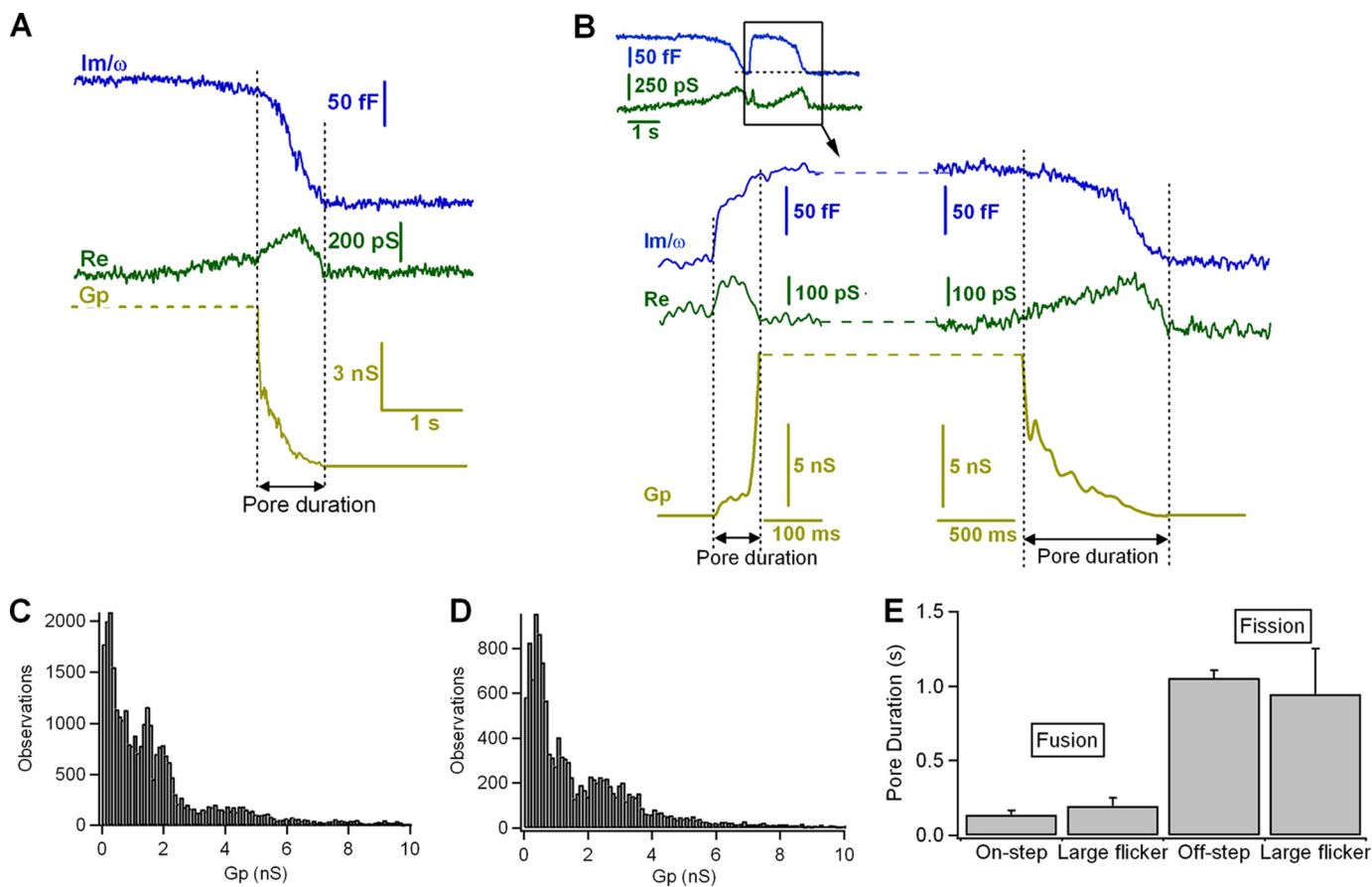
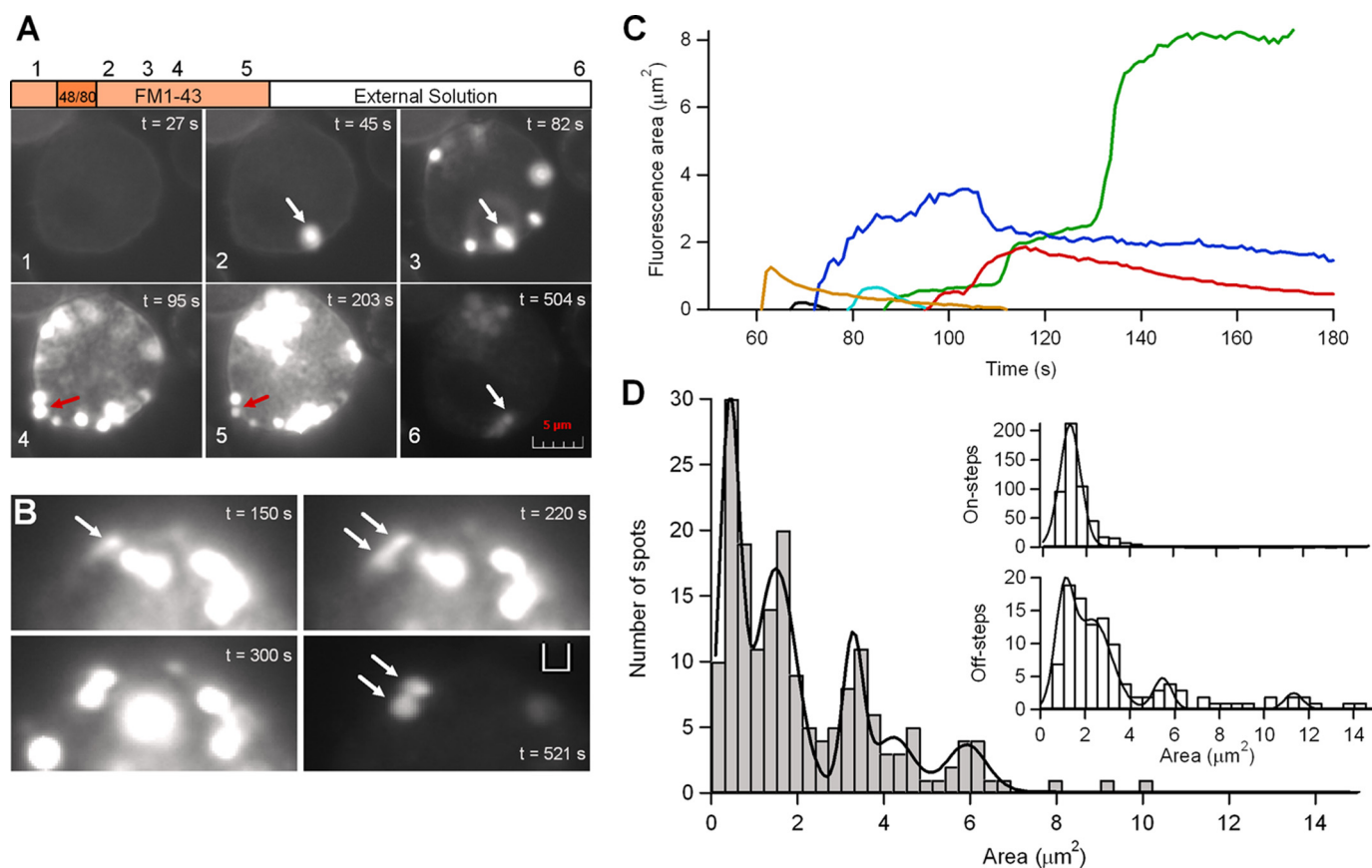


FIGURE 6. **Fusion and fission pores of large reversible events.** A, irreversible endocytic event showing closing of the fission pore. The fission pore conductance was calculated as  $G_p = (Re^2 + Im^2)/Re$ . B, large-capacitance flicker showing two transient increases of the real part ( $Re$ ), indicating the formation of two pores: the fusion and the fission pores. C and D, histograms of  $G_p$  for endocytic events (C) and for large-capacitance flickers (D). E, pore durations of fusion and fission events compared among exocytosis, endocytosis, and large-capacitance flickers. Error bars, S.E.





**FIGURE 7. Exocytosis and endocytosis are visible using FM1-43 fluorescence.** *A*, fluorescence images from one single cell obtained at different stages of the protocol (see "Experimental Procedures"). *Panel 1*, incubation in standard solution with FM1-43. *Panel 2*, 5 s after the application of compound 48/80, exocytosis starts. *Panels 3–5*, degranulation progresses; some spots abruptly can grow in size (white arrow), and others, after reaching a maximal fluorescence, start to decrease both in brightness and size (red arrow). *Panel 6*, after washout, the remaining fluorescence is the result of FM1-43 trapped in the fraction of membrane internalized by endocytosis and/or the FM1-43-stained dense cores retrieved by endocytosis. Scale bar, 1  $\mu\text{m}$ . *B*, time series showing an enlarged portion of an isolated mast cell bathed in solution with 4  $\mu\text{M}$  FM1-43 and stimulated with compound 48/80, as in *A*. One spot abruptly doubles its size after stimulation (white arrows), indicating that one granule fused to the plasma membrane, and another granule fused with that granule. After washing out the external fluorophore, the spot persisted whereas the rest of spots almost disappeared ( $t = 521$  s). *C*, traces showing the fluorescence area over the time (during degranulation) of six individual spots from a single cell stimulated with compound 48/80. In this example, three spots reduced both its area and brightness below the detection threshold, suggesting release of dense cores from the fused granules, whereas three other spots were each several times bigger than the other three. The spots increased its area twice (red line), three times (blue line), or even more (green line). *D*, histogram of maximal fluorescence areas of 181 spots from 24 cells after stimulation with compound 48/80. The distribution is fit to multiple Gaussians (smooth line) with peaks at 0.3, 1.4, 3.1, and 5.8. As many of the spots overlapped during the onset of the degranulation, it was often impossible to discriminate when a spot grew or overlapped spatially with other different spots, so that, likely the maximal fluorescence area from each spot could be underestimated. The insets show histograms of areas corresponding to on- and off-steps events during capacitance measurements in intact mast cells stimulated with compound 48/80. The off-step histogram was fit by a set of Gaussians with peaks at 1.1, 2.4, 5.5, and 11.

courses of these capacitance flickers were indistinguishable from the pores that resulted from irreversible exocytosis and endocytosis events.

**Exocytosis and Endocytosis Can Be Observed in Intact Mast Cells Using the Fluorescent Dye FM1-43**—In resting mast cells exposed to FM1-43, only the surface membrane was stained with dye (Fig. 7A). Stimulation with compound 48/80 caused discrete fluorescent spots, each about the size of a secretory granule (Fig. 7, A and B, and supplemental Videos 1 and 2). Most fluorescent spots appeared quickly, and some spots showed abrupt doublings or triplings in size during the time course of recording (Fig. 7C), indicating compound exocytosis (17). Exocytosis started in the most peripherally located granules, and the spots were initially distributed randomly around the equator of the cell; then, the fluorescence areas were spreading progressively toward the cell interior and sideward. FM dyes typically stain only membranes; but in pituitary lac-

totroph, the entire dense core secretory granule stains with FM1-43 (35). Surely, this property is also present in mast cells. The total fluorescence increase of mast cells greatly exceeded the rise in membrane capacitance recorded with the patch pipette. Capacitance increased an average of 24% in intact cells stimulated with compound 48/80, yet integrated fluorescence in these cells increased 11.6-fold more, by an average of 280%.

The secretory granule size expressed in fluorescence spots area can be compared directly with the area of capacitance steps (Fig. 7D). The histogram of maximal fluorescence areas shows clear spaced peaks at 0.3, 1.4, 3.1, 4.1, and 5.8  $\mu\text{m}^2$ . Estimates of the amount of the area from each capacitance on-step (assuming a specific membrane capacitance of 10  $\text{fF}\cdot\mu\text{m}^{-2}$  of membrane) provide a distribution of secretory granule area that is well fit to a Gaussian, whose peak, centered at 1.03  $\mu\text{m}^2$ , we attribute to the area of a single vesicle. This value is close to the second peak of the fluorescence distribution (1.40  $\mu\text{m}^2$ ). Inter-

## Granule Recapture in Intact Mast Cells

estingly, the following peaks seem to correspond to multiples of 1.4, suggesting that spots were quantal in their distribution of fluorescence areas, and thus higher order peaks largely correspond to the fusion of multiple vesicles. Approximately 30% of spots have a fluorescence area that corresponds to the first peak in the distribution. This includes a very small area ( $0.3 \mu\text{m}^2$ ) to be detected by capacitance measurements (resolution  $>0.5 \mu\text{m}^2$ ). These fluorescent events might represent transient fusion events. Alternatively, they may represent a different population of granules with a relatively less electron dense core.

Most of the fluorescent spots were decreasing in size and brightness for the duration of the experiment, even with FM1-43 still present in the bathing fluid (Fig. 7, A and C), suggesting that the dense cores of secretory granules are susceptible to dissolution and release after exocytosis. When FM1-43 was washed from the chamber, many of spots destained, although some fluorescence signals persisted associated to the same location of the previous spots. Fig. 7B shows a fluorescence spot that doubled its size in a time later suggesting compound exocytosis occurs via fusion of one granule to a granule that is already fused with the plasma membrane. When FM1-43 was removed, the dye could not be washed out from this 2-fold-size spot, suggesting that the two granules already fused sequentially, and their cores had been endocytosed as a single unit. On the other hand, if cores were released one would expect fluorescence appeared after endocytosis as rings, not solid objects, corresponding to the endocytosed secretory membranes and not dense cores, and this could also be observed (supplemental Fig. 1S). The distribution of endosome areas, estimated from the amount of area from each capacitance off-step, is also fit by a set of Gaussians with different areas (Fig. 7D). Although the distribution does not provide a perfect one-to-one correspondence with the fluorescence area peaks, the comparison indicates that endosome areas likely correspond to multiple of a discrete size. Together, these results suggest that after compound exocytosis, the compound membrane of fused granules may be endocytosed.

## DISCUSSION

Exocytosis must be followed by endocytosis, lest the cell surface grow indefinitely. In specialized secretory cells, including neurons and non-neuronal cells, exocytosis and compensatory endocytosis are tightly coupled membrane processes (36–38). In our experiments, the plasma membrane was often observed to be retrieved rapidly following exocytosis in intact mast cells, whereas endocytosis was barely observed in dialyzed cells (Fig. 1). A controversial question remains. What mechanism guarantees that the correct amount of membrane is retrieved after exocytosis? In neuroendocrine cells, secretion can occur through different modes: the kiss-and-run mechanism, by which hormones are released through a narrow fusion pore while larger neuropeptides are retained in the granule core, and the full-collapse mechanism, in which the fusion pore dilation allows the additional release of neuropeptides (39, 40). Experiments performed with whole-cell membrane capacitance assays also support the kiss-and-run mechanism in mast cells (7, 15). Under our experimental conditions, the proportion of capacitance flickers was five times higher in intact than in dia-

lyzed mast cells (Fig. 3D); however, in the literature, the reported frequency of flickers is quite variable under the whole-cell configuration (26, 30, 31). In contrast, following degranulation with GTP $\gamma$ S, the near absence of endocytosis and the growth of the plasma membrane area, up to three times the size, are highly recurrent (28, 31). These facts suggest that the transient fusion mode alone is not an efficient endocytic mechanism to restore normal cell size after exocytosis. Regardless, kiss-and-run fusion may serve as a mechanism to selectively or differentially release secretory granule constituents in mast cells. By amperometry, we observed serotonin release in spike-like form during small-capacitance flickers. These spikes are of lesser quantal charge than those from irreversible on-steps (full-fusion events), supporting the idea of a reduced outflow of transmitters through a narrow and transient fusion pore in these cells (7) as shown in chromaffin cells (41, 42).

If kiss-and-run events cannot solely explain the rapid and tight balance frequently observed between exocytosis and endocytosis in intact mast cells, allowing the rapid retrieval of excess membrane generated by the full fusion of secretory granules, which other endocytic mechanism can restore the resting plasma membrane area levels so quickly? Large-capacitance flickers provide a clue. The recording in Fig. 8 shows that after the consecutive fusion of several distinct secretory granules (steps 2, 3, 4, and 5) that increased the cell membrane capacitance by a total of 57 fF, an off-step in capacitance of 57 fF was observed (step 6). This off-step in capacitance matched, exactly, the sum of the four fusion events (the first event was a transient fusion). A similar example is shown in Fig. 4A. These types of recordings are not new. The phenomena of compound exocytosis and cumulative fusion have been reported previously in mast cells (43), eosinophils (17), pancreatic acini (44), and human neutrophils (45). The proposed explanation is based merely on the ability of secretory granules to form transient (kiss-and-run) connections with the plasma membrane: a peripheral granule undergoes a transient fusion with the plasma membrane and serves as a target for the sequential fusion of granules that are located within deeper layers of the cell. If, at this point, the peripheral granule ends its flicker and is separated from the plasma membrane, a larger structure may be formed, composed of several aggregated granules (43). Our events, however, could be slightly different; large amperometric spikes were observed that were associated with the on-steps, suggesting that full fusion instead of transient fusion occurs. Furthermore, pore conductance analysis indicates that typical fission pores are formed during large off-steps after sequential exocytosis (data not shown). As a consequence, the mechanism that reseals the cavity that is formed by the cumulative fusion of secretory granules is unlikely to be the molecular reverse of fusion. An alternative explanation may be provided by the cavi-capture mechanism, where the granule membrane is maintained in an  $\Omega$  shape yet completely merges with the plasma membrane. In pancreatic acini cells, zymogen granules fused by cumulative fusion maintain their  $\Omega$ -shaped profile for an average of 220 s (44). Retrieving intact secretory granule cavities, as in kiss-and-run endocytosis, is thought to be advantageous to cells because it saves the effort of retrieving vesicle membrane components by molecular sorting (8). Curiously, large-capaci-

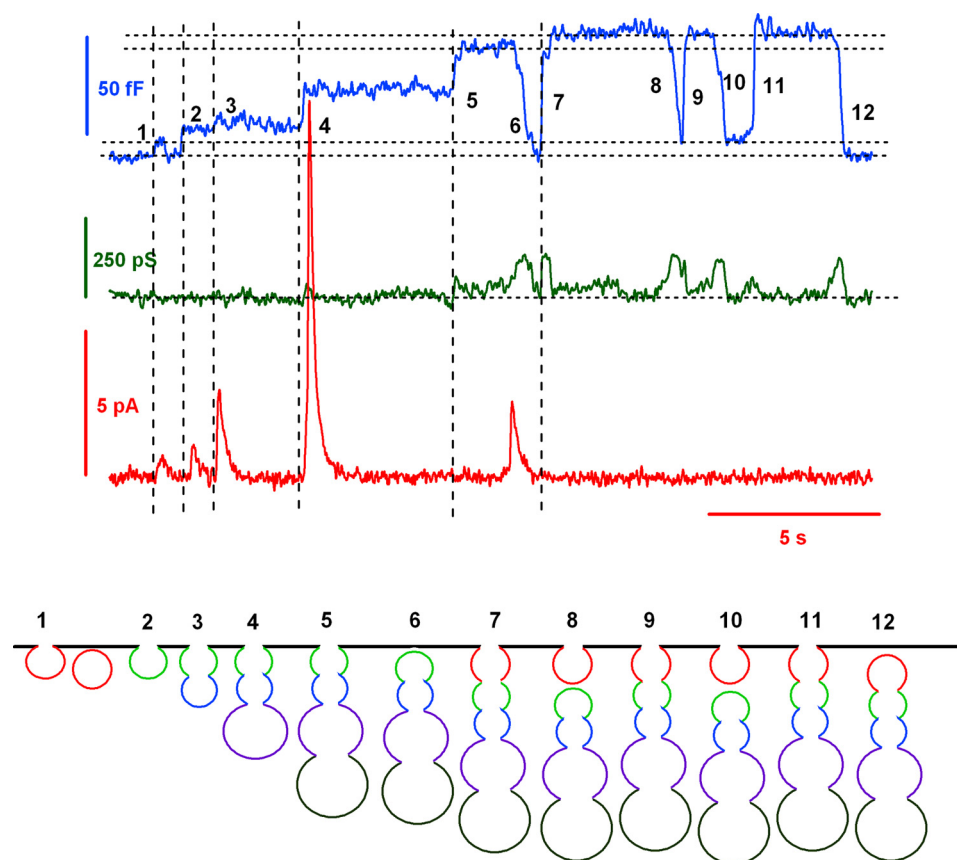


**FIGURE 8. Capacitance and amperometric recordings show that granule exocytosis is followed by compensatory endocytosis.** A possible explanation may be provided by compound cavicapture, a mechanism involving the transient fusion of a large piece of membrane formed by the cumulative fusion of several secretory granules with the cell membrane. Secretory granules can form aggregates of granules through cavicapture. The capacitance trace (blue) shows a small-capacitance flicker (kiss-and-run endocytosis) at 1, followed by four on-steps (steps 2–5), reflecting four secretory granules fusing sequentially with the plasma membrane and releasing their serotonin contents. A first resealing of the entire cavity is observed at step 6 as a large off-step. Later, a larger on-step (step 7) may be interpreted as a new fusion of the granule chain including an additional vesicle (perhaps the first vesicle that fused transiently by the kiss-and-run mechanism). The granule aggregate fused transiently by cavicapture up to three times (steps 7–12) until its final disconnection from the plasma membrane. The cavity tends to increase (steps 11 and 12) or decrease (steps 7 and 8) by membrane flow to or from the cell surface (53). In addition, the second granule of the chain may close instead the first one, leaving the first granule bound to the plasma membrane (step 8).

tance flickers always follow off-steps, even when they occur repeatedly. This type of event suggests that the granules are recaptured as intact units of a chain. From analysis of large-capacitance flickers, we infer that the fusion pore can increase its diameter severalfold and then close again completely. Fusion and fission pores formed during large-capacitance flickers show properties similar to those exhibited by the fusion and fission pores formed during irreversible fusion and fission events (Fig. 6). To our knowledge, these events are the first direct demonstration, by admittance analysis, of the cavicapture mechanism that was proposed by Henkel and Almers (8) and later confirmed by image analysis to occur in insulin-secreting cells (46) and PC12 cells (10). Because these transient events likely correspond to the recapture of the compound cavity formed by several fused granules, we called this type of resealing “compound cavicapture” and the irreversible endocytosis of this organelle compound endocytosis, in analogy to the reverse process of compound exocytosis. Although it seems more likely for large flickers and large off-steps to be formed by the internalization of the aggregated granules generated by sequential exocytosis, large endosomes newly formed could also explain these events. Anyway, live imaging studies of exocytosis and endocytosis with FM1-43 captured morphological

manifestations of compound exocytosis and endocytosis, confirming the functional results obtained by capacitance measurements (Fig. 7). A similar endocytic mechanism has been proposed to occur at synapses. By cell-attached recordings, large off-steps in capacitance were observed to occur later than on-steps of similar size at release sites of the calyx of Held. In this model, compound fusion occurs among small, regular vesicles to form large vesicles. These large vesicles have an increased quantal size and undergo later fusion with the plasma membrane, thereby increasing synaptic strength. These large vesicles are then retrieved by bulk endocytosis (47). In our model, these large structures correspond to granule aggregates formed by the cumulative fusion of single secretory granules instead of by multigranular exocytosis.

Another interesting question is as follows: why do these granule chains flicker before the final internalization? It has been proposed that the sequential mechanism of exocytosis may operate generally in cells in which secretory vesicles are densely packed into multiple layers and in which efficient secretion is necessary. Cumulative fusion has been suggested to reduce the need for the transport of the granule to the plasma membrane and might serve to target the release focally (44). However, an unfavorable consequence is the additional delay



## Granule Recapture in Intact Mast Cells

that is required for the granule contents to be extruded. Following exocytosis in mast cells, granule-associated mediators, such as histamine and serotonin, that are linked with proteoglycans, become soluble immediately and are released, whereas most of structure remains in an insoluble, particulate form (48). Under sequential exocytosis, the extracellular output of soluble mediators from granules that are located more internally may be delayed (note the longer delay between the capacitance on-step and the amperometric spike of the last granule; step 5 in Fig. 8). Likely, the indissoluble core matrix of proteoglycan is retained in the long cavity. Opening and closing of the fusion pore of this compound cavity may be required to expel the larger material of proteoglycans (750–1000 kDa) and associated proteins (undetected by amperometry) at a later time, after the initial fusion and serotonin release.

Cumulative fusion appears to be the major mechanism of secretion in mast cells stimulated with compound 48/80 (49), bee venom (50), or antigens in sensitized cells (51). Under the whole-cell configuration, the mechanism of compound cavi-capture has not been observed. Granules retrieved by cavi-capture have been associated with dynamin, and this recapture was inhibited by GTP $\gamma$ S and peptides that block dynamin function (52). Because GTP $\gamma$ S is the stimulus for inducing degranulation under the whole-cell mode that is commonly used for studying exocytosis by capacitance measurement in mast cells, it is not surprising that off-steps and large-capacitance flickers were rarely observed.

Our results have shown that exocytosis induced by 48/80 in intact mast cells is followed by an endocytic mechanism that can retrieve the exocytosed membrane within seconds. This mechanism is most likely compound endocytosis (and compound cavi-capture), whereby the compound cavity, formed by the cumulative fusion of many secretory granules, is retrieved in a single membrane fission event. Compound endocytosis may be a novel mechanism for efficiently compensating for the membrane excess caused by full-fusion exocytosis.

*Acknowledgment*—We thank Dolores Gutierrez for technical assistance.

### REFERENCES

- Xue, L., and Mei, Y. A. (2011) Synaptic vesicle recycling at the calyx of Held. *Acta Pharmacol. Sin.* **32**, 280–287
- Haucke, V., Neher, E., and Sigrist, S. J. (2011) Protein scaffolds in the coupling of synaptic exocytosis and endocytosis. *Nat. Rev. Neurosci.* **12**, 127–138
- Heuser, J. E., and Reese, T. S. (1973) Evidence for recycling of synaptic vesicle membrane during transmitter release at the frog neuromuscular junction. *J. Cell Biol.* **57**, 315–344
- Slepnev, V. I., and De Camilli, P. (2000) Accessory factors in clathrin-dependent synaptic vesicle endocytosis. *Nat. Rev. Neurosci.* **1**, 161–172
- Royle, S. J., and Lagnado, L. (2003) Endocytosis at the synaptic terminal. *J. Physiol.* **553**, 345–355
- Ceccarelli, B., Hurlbut, W. P., and Mauro, A. (1973) Turnover of transmitter and synaptic vesicles at the frog neuromuscular junction. *J. Cell Biol.* **57**, 499–524
- Alvarez de Toledo, G., Fernández-Chacón, R., and Fernández, J. M. (1993) Release of secretory products during transient vesicle fusion. *Nature* **363**, 554–558
- Henkel, A. W., and Almers, W. (1996) Fast steps in exocytosis and endocytosis studied by capacitance measurements in endocrine cells. *Curr. Opin. Neurobiol.* **6**, 350–357
- Perrais, D., Kleppe, I. C., Taraska, J. W., and Almers, W. (2004) Recapture after exocytosis causes differential retention of protein in granules of bovine chromaffin cells. *J. Physiol.* **560**, 413–428
- Taraska, J. W., and Almers, W. (2004) Bilayers merge even when exocytosis is transient. *Proc. Natl. Acad. Sci. U.S.A.* **101**, 8780–8785
- Richards, D. A., Guatimosim, C., and Betz, W. J. (2000) Two endocytic recycling routes selectively fill two vesicle pools in frog motor nerve terminals. *Neuron* **27**, 551–559
- Takei, K., Mundigl, O., Daniell, L., and De Camilli, P. (1996) The synaptic vesicle cycle: a single vesicle budding step involving clathrin and dynamin. *J. Cell Biol.* **133**, 1237–1250
- Paillart, C., Li, J., Matthews, G., and Sterling, P. (2003) Endocytosis and vesicle recycling at a ribbon synapse. *J. Neurosci.* **23**, 4092–4099
- Neher, E., and Marty, A. (1982) Discrete changes of cell membrane capacitance observed under conditions of enhanced secretion in bovine adrenal chromaffin cells. *Proc. Natl. Acad. Sci. U.S.A.* **79**, 6712–6716
- Fernandez, J. M., Neher, E., and Gomperts, B. D. (1984) Capacitance measurements reveal stepwise fusion events in degranulating mast cells. *Nature* **312**, 453–455
- Breckenridge, L. J., and Almers, W. (1987) Currents through the fusion pore that forms during exocytosis of a secretory vesicle. *Nature* **328**, 814–817
- Scepek, S., and Lindau, M. (1993) Focal exocytosis by eosinophils—compound exocytosis and cumulative fusion. *EMBO J.* **12**, 1811–1817
- Wightman, R. M., Jankowski, J. A., Kennedy, R. T., Kawagoe, K. T., Schroeder, T. J., Leszczyszyn, D. J., Near, J. A., Diliberto, E. J., Jr., and Viveros, O. H. (1991) Temporally resolved catecholamine spikes correspond to single vesicle release from individual chromaffin cells. *Proc. Natl. Acad. Sci. U.S.A.* **88**, 10754–10758
- Oberhauser, A. F., Robinson, I. M., and Fernandez, J. M. (1995) Do caged-Ca<sup>2+</sup> compounds mimic the physiological stimulus for secretion? *J. Physiol. Paris* **89**, 71–75
- Oberhauser, A. F., Robinson, I. M., and Fernandez, J. M. (1996) Simultaneous capacitance and amperometric measurements of exocytosis: a comparison. *Biophys. J.* **71**, 1131–1139
- Chow, R. H., von Rüden, L., and Neher, E. (1992) Delay in vesicle fusion revealed by electrochemical monitoring of single secretory events in adrenal chromaffin cells. *Nature* **356**, 60–63
- Horn, R., and Marty, A. (1988) Muscarinic activation of ionic currents measured by a new whole-cell recording method. *J. Gen. Physiol.* **92**, 145–159
- Alvarez de Toledo, G., and Fernandez, J. M. (1990) Patch-clamp measurements reveal multimodal distribution of granule sizes in rat mast cells. *J. Cell Biol.* **110**, 1033–1039
- Kawagoe, K. T., Zimmerman, J. B., and Wightman, R. M. (1993) Principles of voltammetry and microelectrode surface states. *J. Neurosci. Methods* **48**, 225–240
- Rosenboom, H., and Lindau, M. (1994) Exo-endocytosis and closing of the fission pore during endocytosis in single pituitary nerve terminals internally perfused with high calcium concentrations. *Proc. Natl. Acad. Sci. U.S.A.* **91**, 5267–5271
- Spruce, A. E., Breckenridge, L. J., Lee, A. K., and Almers, W. (1990) Properties of the fusion pore that forms during exocytosis of a mast cell secretory vesicle. *Neuron* **4**, 643–654
- Fernandez, J. M., Lindau, M., and Eckstein, F. (1987) Intracellular stimulation of mast cells with guanine nucleotides mimic antigenic stimulation. *FEBS Lett.* **216**, 89–93
- Oberhauser, A. F., Monck, J. R., and Fernandez, J. M. (1992) Events leading to the opening and closing of the exocytic fusion pore have markedly different temperature dependencies: kinetic analysis of single fusion events in patch-clamped mouse mast cells. *Biophys. J.* **61**, 800–809
- Lindau, M., and Fernandez, J. M. (1986) IgE-mediated degranulation of mast cells does not require opening of ion channels. *Nature* **319**, 150–153
- Oberhauser, A. F., and Fernandez, J. M. (1996) A fusion pore phenotype in mast cells of the ruby-eye mouse. *Proc. Natl. Acad. Sci. U.S.A.* **93**, 14349–14354



31. Fernández-Chacón, R., Alvarez de Toledo, G., Hammer, R. E., and Südhof, T. C. (1999) Analysis of SCAMP1 function in secretory vesicle exocytosis by means of gene targeting in mice. *J. Biol. Chem.* **274**, 32551–32554
32. von Rüden, L., and Neher, E. (1993) A Ca-dependent early step in the release of catecholamines from adrenal chromaffin cells. *Science* **262**, 1061–1065
33. Fesce, R., Grohovaz, F., Valtorta, F., and Meldolesi, J. (1994) Neurotransmitter release: fusion or “kiss-and-run”? *Trends Cell Biol.* **4**, 1–4
34. Cabeza, J. M., Acosta, J., and Alés, E. (2010) Dynamics and regulation of endocytic fission pores: role of calcium and dynamin. *Traffic* **11**, 1579–1590
35. Angleson, J. K., Cochilla, A. J., Kilic, G., Nussinovitch, I., and Betz, W. J. (1999) Regulation of dense core release from neuroendocrine cells revealed by imaging single exocytic events. *Nat. Neurosci.* **2**, 440–446
36. Smith, C., and Neher, E. (1997) Multiple forms of endocytosis in bovine adrenal chromaffin cells. *J. Cell Biol.* **139**, 885–894
37. Artalejo, C. R., Henley, J. R., McNiven, M. A., and Palfrey, H. C. (1995) Rapid endocytosis coupled to exocytosis in adrenal chromaffin cells involves  $\text{Ca}^{2+}$ , GTP, and dynamin but not clathrin. *Proc. Natl. Acad. Sci. U.S.A.* **92**, 8328–8332
38. Gundelfinger, E. D., Kessels, M. M., and Qualmann, B. (2003) Temporal and spatial coordination of exocytosis and endocytosis. *Nat. Rev. Mol. Cell Biol.* **4**, 127–139
39. Fulop, T., Radabaugh, S., and Smith, C. (2005) Activity-dependent differential transmitter release in mouse adrenal chromaffin cells. *J. Neurosci.* **25**, 7324–7332
40. Fulop, T., and Smith, C. (2006) Physiological stimulation regulates the exocytic mode through calcium activation of protein kinase C in mouse chromaffin cells. *Biochem. J.* **399**, 111–119
41. Alés, E., Tabares, L., Poyato, J. M., Valero, V., Lindau, M., and Alvarez de Toledo, G. (1999) High calcium concentrations shift the mode of exocytosis to the kiss-and-run mechanism. *Nat. Cell Biol.* **1**, 40–44
42. Segovia, M., Alés, E., Montes, M. A., Bonifas, I., Jemal, I., Lindau, M., Maximov, A., Südhof, T. C., and Alvarez de Toledo, G. (2010) Push-and-pull regulation of the fusion pore by synaptotagmin-7. *Proc. Natl. Acad. Sci. U.S.A.* **107**, 19032–19037
43. Alvarez de Toledo, G., and Fernandez, J. M. (1990) Compound versus multigranular exocytosis in peritoneal mast cells. *J. Gen. Physiol.* **95**, 397–409
44. Nemoto, T., Kimura, R., Ito, K., Tachikawa, A., Miyashita, Y., Iino, M., and Kasai, H. (2001) Sequential-replenishment mechanism of exocytosis in pancreatic acini. *Nat. Cell Biol.* **3**, 253–258
45. Lollike, K., Lindau, M., Calafat, J., and Borregaard, N. (2002) Compound exocytosis of granules in human neutrophils. *J. Leukoc. Biol.* **71**, 973–980
46. Tsuboi, T., McMahon, H. T., and Rutter, G. A. (2004) Mechanisms of dense core vesicle recapture following “kiss and run” (“cavcapture”) exocytosis in insulin-secreting cells. *J. Biol. Chem.* **279**, 47115–47124
47. He, L., Xue, L., Xu, J., McNeil, B. D., Bai, L., Melicoff, E., Adachi, R., and Wu, L. G. (2009) Compound vesicle fusion increases quantal size and potentiates synaptic transmission. *Nature* **459**, 93–97
48. Kunder, C. A., St John, A. L., Li, G., Leong, K. W., Berwin, B., Staats, H. F., and Abraham, S. N. (2009) Mast cell-derived particles deliver peripheral signals to remote lymph nodes. *J. Exp. Med.* **206**, 2455–2467
49. Röhlich, P., Anderson, P., and Uvnäs, B. (1971) Mast cell degranulation as a process of sequential exocytoses. *Acta Biol. Acad. Sci. Hung.* **22**, 197–213
50. Bloom, G. D., and Haegermark, O. (1967) Studies on morphological changes and histamine release induced by bee venom, *n*-decylamine and hypotonic solutions in rat peritoneal mast cells. *Acta Physiol. Scand.* **71**, 257–269
51. Anderson, P., Slorach, S. A., and Uvnäs, B. (1973) Sequential exocytosis of storage granules during antigen-induced histamine release from sensitized rat mast cells *in vitro*: an electron microscopic study. *Acta Physiol. Scand.* **88**, 359–372
52. Holroyd, P., Lang, T., Wenzel, D., De Camilli, P., and Jahn, R. (2002) Imaging direct, dynamin-dependent recapture of fusing secretory granules on plasma membrane lawns from PC12 cells. *Proc. Natl. Acad. Sci. U.S.A.* **99**, 16806–16811
53. Monck, J. R., Alvarez de Toledo, G., and Fernandez, J. M. (1990). Tension in secretory granule membranes causes extensive membrane transfer through the exocytotic fusion pore. *Proc. Natl. Acad. Sci. U.S.A.* **87**, 7804–7808